PCCP

Cite this: *Phys. Chem. Chem. Phys.*, 2012, **14**, 1728–1734

www.rsc.org/pccp

PAPER

Effects of thermodynamic ensembles and mineral surfaces on interfacial water structure†

Todd R. Zeitler,* Jeffery A. Greathouse and Randall T. Cygan

Received 11th August 2011, Accepted 22nd November 2011
DOI: 10.1039/c2cp22593j

While performing molecular dynamics simulations of water or aqueous solutions in a slab geometry, such as at mineral surfaces, it is important to match bulk water density in the diffuse region of the model system with that expected for the appropriate experimental conditions. Typically, a slab geometry represents parallel surfaces with a variable region of confined water (this region can range in size from a few Ångstroms to many tens of Ångstroms). While constant-pressure simulations usually result in appropriate density values in the bulk diffuse region removed from either surface, constant-volume simulations have also been widely used, sometimes without careful consideration of the method for determining water content. Simulations using two thermodynamic ensembles as well as two methods for calculating the water-accessible volume have been investigated for two distinct silicate surfaces—hydrophilic cristobalite (111) and hydrophobic pyrophyllite (001). In cases where *NPT* simulations are not feasible, a simple geometry-based treatment of the accessible volume can be sufficient to replicate bulk water density far from the surface. However, the use of the Connolly method can be more appropriate in cases where a surface is less well-defined. Specific water–surface interactions (*e.g.*, hydrophobic repulsion) also play a role in determining water content in a confined water simulation. While reported here for planar surfaces, these results can be extended to an interface with any solvent, or to other types of surfaces and geometries.

Introduction

Mineral–water interactions drive our understanding of many environmental processes, including mineral dissolution, solute adsorption, heterogeneous nucleation, and colloid transport. Molecular simulation has become an increasingly useful tool to provide atomistic details for such interfacial processes that may be inaccessible to experiment.[1] Previous studies have shown that substrate structure plays a principal role in these interactions, as it defines the underlying framework for water behavior at mineral interfaces.[2] For example, the dynamics of water at interfaces is known to vary on the Ångstrom scale.[3,4] The structure and behavior of water at a surface varies drastically among minerals, even for different surfaces of a single phase, based on factors such as local charge, surface hydroxyl density, and bulk elemental composition. The presence of steps, kinks, or surface functionalization (hydroxyl groups) further complicates the assignment of available surface sites for adsorption. This challenge extends to the increasingly important simulation studies of mineral–water interfaces, where model input must adhere to experimental results whenever possible.

One of the most well-defined connections to experimental data in these cases is the bulk density of water, which is also an important quantity in the validation of classical water models. However, the density of water at an interface is usually unknown. Without an accurate bulk water density far from the surface in the simulation, the water density at the interface will be in error. This is particularly important for simulations in which two surfaces should be independent of each other (which is not always the case for nanoconfined water, for example[5]). A simple, consistent procedure for defining the water-accessible volume of interfacial systems would allow researchers to properly match the bulk density of the pure water model with that in the diffuse central region of the simulation cell (for simulating surfaces in contact with bulk water), resulting in consistent interfacial structures (including interfacial water density) and energies for comparison.

The *NVT* ensemble (constant number of particles, volume, and temperature) is commonly used in molecular dynamics (MD) simulations of water–surface interactions using periodic slab geometries in which two confining surfaces are exposed to an aqueous region.[2,6,7] In this type of model, it is important to have the correct water density in the bulk diffuse region removed from the interfaces if the surfaces are truly noninteracting.

Sandia National Laboratories, Albuquerque, New Mexico 87185-0754, USA. E-mail: tzeitle@sandia.gov
† Electronic supplementary information (ESI) available. See DOI: 10.1039/c2cp22593j

This density should replicate that of the pure water model, which has usually been parameterized to match experimental values. Without carefully determining the water-accessible volume in such a model, the bulk density of water may not reproduce the experimental value, and this will subsequently affect the structure of water at the mineral interface. Any effect on structure will be particularly important when this type of study is extended to investigate adsorption phenomena. Simulations of aqueous solutions at mineral surfaces would necessarily require a match of the solution density in the diffuse region to experimental values.

Some studies have made use of *NVT* simulations with a large vacuum gap such that only one surface is in contact with water—the water region is permitted to expand into the vacuum gap, introducing an additional degree of freedom to allow for equilibration of water at the surface.[8,9] While this methodology gives reasonable "bulk" water density values at large distances from the solid–liquid and liquid–vapor interfaces, the vacuum may introduce a false representation of the system to be modeled. Also, the statistics of interest (*e.g.*, water density at the solid–liquid interface) are halved because only one interface is simulated. The case of solid–liquid–vapor–liquid–solid layering[10] is fundamentally equivalent to the "vacuum" case examined here, though the resulting structure of the former would have two water–vapor interfaces equivalent to the single water–vapor interface of the "vacuum model."

Still other studies have used *NPT* (constant pressure) ensembles (with water confined between two surfaces) which allow the simulation cell to change size to accommodate the user-prescribed water content.[11] For a sufficiently large aqueous region, the bulk water density should be reached in the diffuse region. By allowing the simulation cell to change size, simulations using the *NPT* ensemble should give the ideal result with respect to bulk liquid density in the diffuse central region of the simulation cell.

For some *NVT* studies, a "geometric" approach is sometimes used, where the water-accessible region is estimated based on the positions of surface atoms.[2,6,7,12] If the geometry of the surface is uniform (*e.g.*, a high symmetry phase or a clay basal plane), then this calculation is relatively straightforward and a reasonable estimate for the accessible volume is expected. However, when the geometry of the surface is complicated (*e.g.*, surface hydroxyls or kinks), an alternative method may be more accurate. One method for determining accessible volume for complicated structures is the Connolly surface determination, which has been used previously for determining solvent-accessible sites around micelles.[13] In this method, the accessible surface area is estimated by tabulating close contacts between a probe atom of finite radius and the van der Waals radii of surface atoms.

In this study we have investigated the effects of two thermodynamic ensembles (*NVT* and *NPT*) as well as two methods for determining water content on the interfacial structure and bulk water density in slab geometry models of two contrasting types of mineral–water interfaces, those involving the hydrophobic pyrophyllite (001) surface and the hydrophilic cristobalite (111) surface.

Cristobalite is a mineral with chemical formula SiO_2 and is comprised of structural SiO_4 tetrahedra connected *via* bridging oxygen atoms (each oxygen connects two tetrahedra). The high-temperature form, β-cristobalite (hereafter referred to as simply "cristobalite"), has a cubic structure with an experimentally measured cell parameter of 7.16 Å.[14] The (111) surface of cristobalite exposed to a wet environment is hydrophilic, and is defined by inverted siloxane rings with each surface silicon atom bonded to a single hydroxyl group and three bridging oxygen atoms. On an optimized "dry" surface, a distance of about 5 Å separates oxygen atoms on adjacent hydroxyl groups.[15] Pyrophyllite is a phyllosilicate mineral with chemical formula $Al_2Si_4O_{10}(OH)_2$ and forms electrostatically neutral, layered sheets usually with a triclinic ($C\bar{1}$) crystal structure.[16] Each layer is formed by an alumina sheet sandwiched between two silica sheets. Because the hydroxyl groups of pyrophyllite are internal to the octahedral aluminium atoms, the interlayer (001) basal surface is composed solely of siloxane rings and is relatively hydrophobic. Our choice of surfaces represents extreme cases for neutral surfaces. Comparing water structure near the pyrophyllite surface with that of a charged surface of a similar layered mineral (*e.g.*, muscovite) would be biased due to the net negative charge on the layers and the presence of counterions near the charged surface.

Computational details

Models for the cristobalite (111) and pyrophyllite (001) surfaces were constructed using published crystal structures.[14,16] Using the Materials Studio (Accelrys, Inc.) software package, two surfaces were cleaved for each mineral while simultaneously introducing a vacuum gap of about 40 Å. Each structure was then replicated in the *x*- and *y*-directions such that each cell parameter was at least 20 Å (Table 1). Three-dimensional periodic boundary conditions were used to effectively simulate an infinite number of parallel slabs.

For cristobalite, cleaving along the (111) plane leaves one non-bridging oxygen atom bonded to each silicon atom on one surface and a second surface of exclusively three-coordinated silicon atoms. Properly coordinated surfaces were created to represent the dissociative adsorption of water: one hydrogen atom was attached to each of the non-bridging oxygen atoms, and a hydroxyl group was attached to each three-coordinated

Table 1 Structural parameters for cristobalite and pyrophyllite

	a/Å	*b*/Å	*c*/Å	α/°	β/°	γ/°	Geometric surface area[a]/Å^2 per surface	# H_2O
Cristobalite[b]	7.160	7.160	7.160	90.00	90.00	90.00	—	—
Pyrophyllite[b]	5.160	8.966	9.347	91.18	100.46	89.64	—	—
Cristobalite (111)[c]	20.559	20.559	59.492	90.00	90.00	120.00	366.1	434
Pyrophyllite (001)[c]	25.894	26.969	74.114	90.00	90.00	89.85	698.3	863

[a] Surface area based on cell parameters. [b] Experimental bulk structure. [c] Initial simulated surface structure ("geometry" structure).

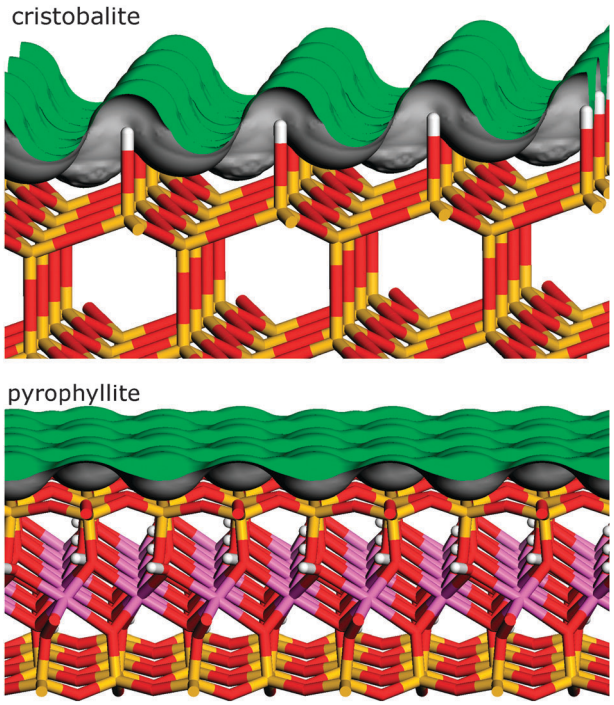

Fig. 1 Connolly surface of cristobalite (111) (top) plotted above its structural model, and of pyrophyllite (001) (bottom) plotted above its structural model (red = O, yellow = Si, white = H, pink = Al, green = Connolly surface).

silicon atom, therefore maintaining charge neutrality (Fig. 1). A classical geometry optimization of the surface hydroxyl groups was performed using Clayff[17] parameters in order to have a relaxed surface structure for later calculations. Because pyrophyllite has perfect cleavage in the (001) plane, no bonds were broken during creation of the (001) surface. For each mineral, this cleavage procedure yielded two identical surfaces.

Molecular dynamics simulations were performed using the Nosé–Hoover thermostat implemented in the LAMMPS[18] code with a relaxation time of 0.1 ps. For *NPT* simulations with a Nosé–Hoover barostat, a barostatic relaxation time of 1.5 ps was used. Interatomic interactions include van der Waals and electrostatic terms, and long-range electrostatics were evaluated every 1.0 fs *via* an augmented Ewald summation[19] with a precision of 1.0×10^{-4}. This "Ewald/n" version (implemented in LAMMPS for nonorthogonal simulation boxes) also acts on van der Waals interactions outside the short-range cutoff. Short-range interactions were evaluated every 0.5 fs with a real-space cutoff of 10.0 Å. Force field parameters were taken from Clayff,[17] which has implemented the SPC[20] water model with harmonic bond stretch and bond bend potentials. Clayff, which allows complete atomic motions, has been successfully applied in classical simulations of water–mineral interfaces.[2,21,22] All MD simulations were performed at 298 K, and at 0.1 MPa for the NPT ensemble.

The number of water molecules in the aqueous region between the two surfaces was first calculated based on a geometric definition of the mineral surface. The water-accessible volume was defined by the geometric surface area (Table 1) and the perpendicular distance between hydroxyl oxygen (cristobalite) or surface oxygen (pyrophyllite) atoms. The van der Waals diameter of an oxygen atom (3.04 Å)[23] was taken into account in both cases. From the calculated volume, the appropriate number of water molecules (Table 1) was calculated such that an overall density of 1.0 g cm^{-3} was achieved for the entire aqueous region. *NVT* simulations using this configuration are referred to below as the "geometry" case.

A second method of calculating water-accessible volume is through the Connolly surface method, as described above.[13,24] Based on this volume and the bulk density of water (1.0 g cm^{-3}), the appropriate number of water molecules needed to properly saturate the aqueous region is calculated. The critical parameter in the Connolly surface method is the probe size, which can be related to the size of the species of interest (in this case, a water molecule) and/or optimized to exclude void space in the bulk structure. Based on a density of 1.0 g cm^{-3}, each water molecule occupies a volume of 29.91 $Å^3$. Assuming this volume is that of a cube inscribed by a spherical particle, this particle has a radius of 1.55 Å, which we use as the Connolly probe radius for both mineral systems. In the case of cristobalite, the probe radius is small enough such that inaccessible volume in the mineral substrate could be included in the accessible volume calculation if care is not taken to explicitly exclude these inaccessible regions.

To adequately compare the two methods of calculating the water-accessible volume, *NVT* simulations with the same number of water molecules are needed. However, the accessible volumes (and thus the number of water molecules to be included in the simulation) calculated *via* the two methods are not equal. By changing the gap distance between the two surfaces (a reduction by 2.4 Å for cristobalite and 0.8 Å for pyrophyllite), the water-accessible volume of the "Connolly" structure was made equal to that of the "geometry" case.

Water molecules were inserted into the vacuum gap in a regular lattice, simulated at 1000 K, and then quenched to 298 K while the atoms of the mineral structure were completely constrained. Two types of subsequent simulations (*NVT* and *NPT*) were performed beginning from the final configuration of the quench run. In each case, the simulation was 11.2 ns in time length, with structural data collected at 100 fs intervals over the final 10 ns (10^5 configurations). In the *NPT* simulation, only the cell parameter perpendicular to the surface was allowed to vary. *NPT* simulations were performed using both the "geometry" and "Connolly" initial structures. For each of the two materials, the average cell parameter of the *NPT* simulations agreed to within 0.2 Å, so the equilibrium structures were considered equivalent and only the results of the simulation beginning from the "geometry" initial configuration are presented here (denoted "*NPT*").

Finally, a fourth simulation was run where the initial configuration was that of the "geometry" case with an additional 50 Å vacuum gap inserted such that all water molecules saturated only one surface. An *NVT* simulation following the procedure above was run for this configuration and the results are denoted as "vacuum."

Results and discussion

The two minerals exhibit very different Connolly surfaces: cristobalite (111) has a nonuniform "egg-crate" structure due to silanol groups that protrude into the interfacial region,

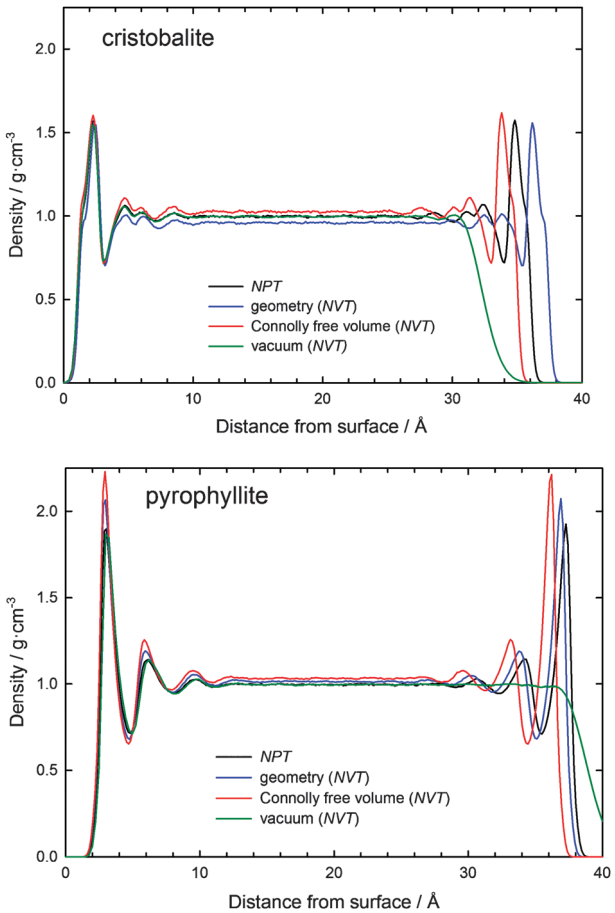

Fig. 2 Water density profiles (based on oxygen positions) as a function of distance from the surface for cristobalite (111) (top) and pyrophyllite (001) (bottom) based on *NVT* and *NPT* ensembles. The surfaces are defined by the mean positions of oxygen in surface hydroxyl groups for cristobalite (111) and bridging surface oxygen for pyrophyllite (001).

while pyrophyllite has a more planar, slightly dimpled structure defined by bridging oxygen atoms that comprise the siloxane ring structure of the basal surface (Fig. 1).

Calculated water density profiles (from the position of oxygen in each water molecule) in the direction perpendicular to the surface for the resulting structures of cristobalite (111) and pyrophyllite (001) are plotted in Fig. 2. The *NPT* plots of Fig. 2 were generated by scaling the fractional atomic coordinates by the average simulation cell size over the final 10 ns of simulation time. The mean water density in the diffuse region was calculated over 10 Å at the center of each box and is compared to the bulk density of water from an *NPT* simulation of 434 H_2O molecules (Table 2). For the "vacuum" case, bulk density was calculated over the region 12–22 Å from the surface.

The water structure at the cristobalite (111) surface is characteristic of a hydrophilic surface with a rhombic array of hydroxyl groups (water oxygen peaks at about 2.3 Å and 4.7 Å from the surface), similar to $Mg(OH)_2$ brucite (001) or $Al(OH)_3$ gibbsite (001).[2] One feature not observed in atomic profiles of brucite or gibbsite is the shoulder in the first peak, which indicates that some water molecules in the first interfacial layer are preferentially adsorbed at approximately 1.7 Å. This is not surprising given that hydroxyl groups on the cristobalite (111) surface are about 5 Å apart, while on the (001) surfaces of brucite and gibbsite the hydroxyl separations are about 3 Å. This additional space allows for penetration of water molecules, and underlines the challenge of properly defining the accessible volume when simulating an irregular surface so that the bulk density of water is correctly modeled in the diffuse region of the simulation cell.

The water structure at the pyrophyllite (001) surface is characteristic of a relatively hydrophobic surface with no surface hydroxyl groups (water oxygen peaks at about 3 Å and 6 Å) similar to talc.[2] The hydrophobicity of the surface is reflected in the greater separation of the first water layer from the surface as well as the ~3 Å separation between the first two layers. The greater number of features in the cristobalite profile near the surface suggests a stronger local mineral–water interaction (*i.e.*, structuring), as expected.[2]

In Fig. 3, density profiles at the water–mineral interface are shown along with snapshots of the corresponding structures from the *NPT* simulations. There is a stronger interaction of water with the cristobalite surface as evidenced by the overlap of water species and surface hydrogen, compared to the excluded volume at the surface of pyrophyllite. This difference can be attributed to the relative hydrophobicity of pyrophyllite (001). The peak positions for H (H_2O) and O (H_2O) for pyrophyllite are nearly coincident and relatively evenly spaced, which indicates the presence of ordered water. However, for cristobalite, peak positions are separated, indicating a water orientation that promotes hydrogen bonding to the surface.

The density of pure water in an *NPT* simulation of SPC water is 0.997 g cm^{-3}. This water density can be considered the target density for the diffuse central region and is obtained in the central diffuse regions in *NPT* simulations of both minerals (Table 2). The variable cell volume in the *NPT* ensemble allows the water density in the diffuse region to more closely

Table 2 Comparison of simulation results, including water density at the center of simulation cell (ρ_c), *c*-parameter, and maximum water density (ρ_{max}) at the first peak in the density profile

Material	Method	ρ_c/g cm^{-3}	Std. dev. ρ_c/g cm^{-3}	% diff. ρ_c	*c*-parameter/Å	ρ_{max}/g cm^{-3}	% diff ρ_{max}
Cristobalite	*NPT*	0.997	0.004	—	58.13	1.57	—
	Geometry (*NVT*)	0.959	0.004	−3.8	59.49	1.56	−1.0
	Connolly (*NVT*)	1.025	0.004	2.8	57.10	1.62	2.9
	Vacuum (*NVT*)	0.996	0.003	−0.1	109.49	1.55	−1.8
Pyrophyllite	*NPT*	0.996	0.002	—	74.82	1.92	—
	Geometry (*NVT*)	1.013	0.002	1.7	74.11	2.07	7.7
	Connolly (*NVT*)	1.032	0.003	3.5	73.32	2.23	16
	Vacuum (*NVT*)	0.996	0.003	−0.1	124.11	1.87	−3.0
H_2O	*NPT*	0.997	0.003	—	—	—	—

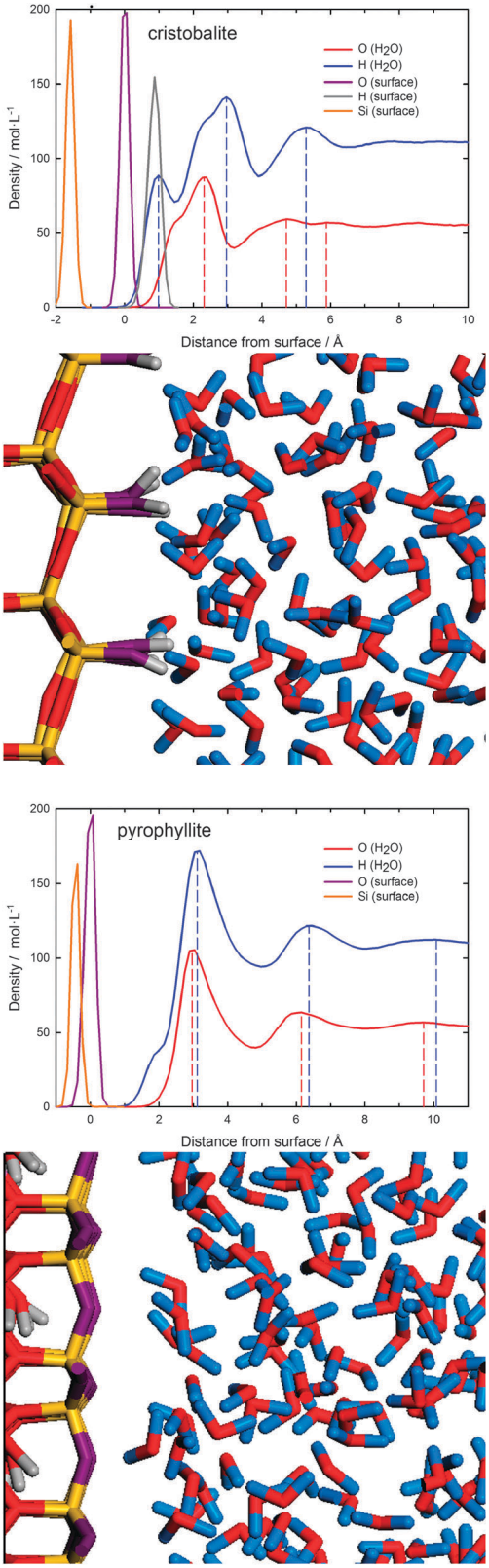

Fig. 3 Density profile and structure near the surface of cristobalite (111) (top) and pyrophyllite (001) (bottom) from the *NPT* simulation based on 10^5 configurations over 10 ns. Density values for water species have units of mol L^{-1}, while surface species are scaled arbitrarily for ease of viewing. Colors used in the density plot correspond to those of molecules in the structure shown in the figure.

match that of bulk water. The density of bulk water in the "vacuum" *NVT* simulation also compares well with the density of pure water. In this case, the lack of confinement (due to the vacuum gap) allows the correct bulk density of water to be reached for water on one surface. Both *NPT* and "vacuum" simulations yield accurate density values, indicating that the system is well-equilibrated. This gives greater confidence in the interfacial water structure derived from these simulations (Fig. 3).

For cristobalite, starting from the "geometry" structure, the cell contracts during *NPT* simulation, indicating a larger volume in the geometry-*NVT* case, given the number of water molecules included in the simulation cell. The geometry method for calculating water-accessible volume fails to account for some of the cell volume that is accessible to water, resulting in a smaller water density. Another possible explanation of the contraction would be an overall increase in water density at the surface such that the entire cell contracts to maintain the model bulk density in the diffuse region. However, this can be discounted by noting that the interfacial water has a lower density than the bulk—the average density in the region within 10 Å of the surface (which consists of both high and low density regions) is 0.89 g cm^{-3}. Thus if a change in density at the interface was the cause for a change in size of the simulation cell, we would expect an *expansion* of the simulation cell under subsequent *NPT* conditions. The cell contraction must be due to underestimation of the accessible volume with the "geometry" method. Additional evidence is found in Fig. 1, where the corrugated cristobalite surface allows for additional accessible volume in the same region as surface silanol groups. Comparing the water densities in the diffuse central region of the simulation cell, the constraints of the *NVT* "geometry" simulation have resulted in a density difference of 3.8% compared to the *NPT* case (Table 2).

Turning to the results of the "Connolly" simulation for cristobalite, the cell expands during *NPT* simulation due to a smaller initial cell size than required for the number of water molecules included in the simulation cell (*i.e.*, a larger water density). The accessible volume from the Connolly method takes into account volume between surface silanol groups which is neglected in the "geometry" method. The extent to which this additional accessible volume is correctly counted could be optimized by including information about the librational dynamics of surface silanol groups and hydrogen bonding at the surface, though an accurate, systematic way of doing this *a priori* is not immediately clear, and any impact on the results shown here is unlikely. In this case, the Connolly method applied to the cristobalite (111) surface leads to a density difference of 2.8% in the diffuse region as compared to the *NPT* case (Table 2), which makes it a more accurate method for determining water content than the "geometry" method for this surface.

For both the "geometry" and Connolly initial configurations of the pyrophyllite (001) surface, the cell expands during *NPT* simulation, indicating that the initial simulation cell was too small for the number of water molecules included. This can be attributed to the hydrophobic nature of the pyrophyllite surface which creates a greater excluded volume at the surface, resulting in a lower water density. Because these two methods

do not consider *a priori* the chemical nature of the water–surface interaction (in this case, repulsion), it stands to reason that both could overestimate the accessible volume at the surface in a structure where there is significant excluded volume (*i.e.*, by assuming that the additional water molecules would have access to the excluded volume). A comparison of the water density profiles in Fig. 3 demonstrates the effect of surface hydrophobicity. The cristobalite (111) surface shows a shoulder at 1.7 Å and a peak at 2.3 Å. For the pyrophyllite surface, there is a single peak at 3.0 Å with almost no density within 2 Å of the mineral surface. Hydrophobicity is not included in the Connolly method, as it is based only on the van der Waals radii of hard spheres. The known hydrophobicity of the pyrophyllite basal surface is replicated with the current model even though no specific interactions related to hydrophobicity are included (*i.e.*, the hydrophobicity is fully accounted by van der Waals and electrostatic interactions).

Comparing the "geometry" and "Connolly" *NVT* simulations with the *NPT* simulations for both materials, we see that the change in the height of the principal atomic density peaks (*i.e.*, the maximum density in Fig. 2) is more dramatic for pyrophyllite. For the "Connolly" simulation, the first peak is 16% greater than the same peak for the *NPT* simulation (for "geometry," it is 7.7% higher). In contrast, the peak heights in the cristobalite density profile are relatively constant (2.9% increase for the "Connolly" case and 1.0% reduction for the "geometry" case). This suggests a consistent overestimation of water density at the pyrophyllite interface compared to cristobalite. The constraint of fixed volume in *NVT* simulations leads to an overall higher water density in the diffuse region as well as at the first three principal water peaks at the surface. Because the density difference is only 1.7–3.5% in the diffuse region, but 7.7–16% at the first peak, there must be an additional effect of the immediate surface (likely due to hydrophobicity) on the water density at the pyrophyllite surface. While the *atomic* density peak positions do not differ much among the *NVT* and *NPT* simulations (Fig. S1 and S2 of ESI†), clearly there are significant differences in the structure of water at the surface based on maximum density values.

For both surfaces, the Connolly method overestimates the water-accessible volume. This could be due to a relatively small probe size chosen for calculating accessible volume such that inaccessible volume is included along with truly accessible volume. Separate calculations (data not shown) for smaller probe sizes indeed show a greater accessible volume (with a greater effect percentage-wise for the cristobalite surface as compared to the pyrophyllite surface). However, there is no physical rationale for increasing the probe size above 1.55 Å in order to decrease the calculated accessible volume (the kinetic radius of H_2O is 1.32 Å[25] and the equilibrium H–H distance for the water SPC model is about 1.63 Å[20]). In any case, there is no way to know *a priori* the optimal probe size to use to calculate the accessible volume that can reproduce the bulk density of water in the diffuse region of an *NPT* simulation.

It is possible that thermal effects contribute to the volume, such that some of the accessible volume calculated by the Connolly method (on the optimized surface with all silanol groups dispersed in the same direction) is inaccessible during dynamic simulations (where the structure of the surface has now changed). We would expect this effect to be greater for the cristobalite surface because movement of isolated silanol groups could hinder the approach of water molecules. However, because the difference in density is greater for pyrophyllite (the effect on bulk density is 3.5% for pyrophyllite and 2.8% for cristobalite), we must conclude that this is not the dominant reason for the discrepancy and that the excluded volume (due to the hydrophobicity of the pyrophyllite surface) is the dominant effect. Because it is not possible to know the extent of this effect without performing an *NPT* simulation, there is some risk in using the Connolly method to determine water content for an *NVT* simulation. Based on the results presented here, for a more complicated surface geometry, the Connolly method works better, though specific surface features (*e.g.*, due to hydrophobicity or local charge structure) may also contribute to its effectiveness. In summary, it is important that molecular simulations incorporate appropriate water content and consider accessible volume to accurately predict water structure and behavior at solid–water interfaces.

Conclusion

While an *NPT* simulation using molecular dynamics usually guarantees that the appropriate water density will be achieved for systems with slab geometries, in some cases (*e.g.*, rigid substrate) it is not feasible to perform a full *NPT* simulation. An *NVT* simulation with a large vacuum gap also results in an accurate density in the diffuse region removed from the surface, but has the limitation of yielding only a single simulated surface. However, to simulate water confined between two isolated surfaces, the water content must be calculated to replicate the bulk model density in the central region of the cell. While in some cases a simple geometry argument may be sufficient for calculating accessible volume, for complicated surfaces (*e.g.*, those with kinks or hydroxyl groups), using the Connolly method can result in increased accuracy. However, because neither of the two methods for calculating accessible volume takes into account specific water–surface interactions (*e.g.*, hydrophobicity) *a priori*, there are limitations to their usefulness, and their implementation in fixed-volume molecular simulations should be monitored carefully.

Acknowledgements

We gratefully acknowledge three reviewers who helped improve the manuscript. This work is supported by the US Department of Energy, Office of Basic Energy Sciences, Geosciences Research. Sandia National Laboratories is a multi-program laboratory managed and operated by Sandia Corporation, a wholly owned subsidiary of Lockheed Martin Corporation, for the US Department of Energy's National Nuclear Security Administration under contract DE-AC04-94AL85000.

References

1 S. Nangia and B. Garrison, *Theor. Chem. Acc.*, 2010, **127**, 271–284.
2 J. W. Wang, A. G. Kalinichev and R. J. Kirkpatrick, *Geochim. Cosmochim. Acta*, 2006, **70**, 562–582.

3 P. Kumar, S. V. Buldyrev, F. W. Starr, N. Giovambattista and H. E. Stanley, *Phys. Rev. E: Stat. Phys., Plasmas, Fluids, Relat. Interdiscip. Top.*, 2005, **72**, 051503.
4 L. M. Liu, C. J. Zhang, G. Thornton and A. Michaelides, *Phys. Rev. B: Condens. Matter*, 2010, **82**, 161415(R).
5 H. Thompson, A. K. Soper, M. A. Ricci, F. Bruni and N. T. Skipper, *J. Phys. Chem. B*, 2007, **111**, 5610–5620.
6 S. Kerisit, C. X. Liu and E. S. Ilton, *Geochim. Cosmochim. Acta*, 2008, **72**, 1481–1497.
7 J. A. Greathouse, R. J. O'Brien, G. Bemis and R. T. Pabalan, *J. Phys. Chem. B*, 2002, **106**, 1646–1655.
8 J. W. Wang, A. G. Kalinichev, R. J. Kirkpatrick and R. T. Cygan, *J. Phys. Chem. B*, 2005, **109**, 15893.
9 J. A. Greathouse and R. T. Cygan, *Phys. Chem. Chem. Phys.*, 2005, **7**, 3580–3586.
10 S. Kerisit, D. J. Cooke, A. Marmier and S. C. Parker, *Chem. Commun.*, 2005, 3027–3029.
11 S. H. Garofalini, T. S. Mahadevan, S. Y. Xu and G. W. Scherer, *ChemPhysChem*, 2008, **9**, 1997–2001.
12 A. A. Skelton, D. J. Wesolowski and P. T. Cummings, *Langmuir*, 2011, **27**, 8700–8709.
13 H. Kuhn, B. Breitzke and H. Rehage, *Colloid Polym. Sci.*, 1998, **276**, 824–832.
14 T. F. W. Barth, *Am. J. Sci.*, 1932, **23**(s5), 350–356.
15 J. J. Yang, S. Meng, L. F. Xu and E. G. Wang, *Phys. Rev. B: Condens. Matter*, 2005, **71**, 035413.
16 J. H. Lee and S. Guggenheim, *Am. Mineral.*, 1981, **66**, 350–357.
17 R. T. Cygan, J.-J. Liang and A. G. Kalinichev, *J. Phys. Chem. B*, 2004, **108**, 1255–1266.
18 S. Plimpton, *J. Comput. Phys.*, 1995, **117**, 1–19.
19 P. J. in't Veld, A. E. Ismail and G. S. Grest, *J. Chem. Phys.*, 2007, **127**, 144711.
20 H. J. C. Berendsen, J. C. M. Postma, W. F. van Gunsteren and J. Hermans, in *Intermolecular Forces*, ed. B. Pullman, Dordrecht, Riedel, Amsterdam, The Netherlands, 1981, pp. 331–342.
21 N. W. Ockwig, J. A. Greathouse, J. S. Durkin, R. T. Cygan, L. L. Daemen and T. M. Nenoff, *J. Am. Chem. Soc.*, 2009, **131**, 8155–8162.
22 J. L. Suter, P. V. Coveney, H. C. Greenwell and M. A. Thyveetil, *J. Phys. Chem. C*, 2007, **111**, 8248–8259.
23 A. Bondi, *J. Phys. Chem.*, 1964, **68**, 441–451.
24 M. L. Connolly, *Science*, 1983, **221**, 709–713.
25 J. R. Li, R. J. Kuppler and H. C. Zhou, *Chem. Soc. Rev.*, 2009, **38**, 1477–1504.

